

We are IntechOpen, the world's leading publisher of Open Access books Built by scientists, for scientists

6,900

Open access books available

186,000

International authors and editors

200M

Downloads

Our authors are among the

154

Countries delivered to

TOP 1%

most cited scientists

12.2%

Contributors from top 500 universities



WEB OF SCIENCE™

Selection of our books indexed in the Book Citation Index
in Web of Science™ Core Collection (BKCI)

Interested in publishing with us?
Contact book.department@intechopen.com

Numbers displayed above are based on latest data collected.
For more information visit www.intechopen.com



Organic-Organic Semiconductor Interfaces for Molecular Electronic Devices

Ji-Seon Kim¹ and Craig Murphy²

¹*Department of Physics & Centre for Plastic Electronics, Imperial College London,*

²*National Physical Laboratory (NPL)
United Kingdom*

1. Introduction

Molecular (Plastic) electronics encompasses the materials science, chemistry and physics of molecular electronic materials and the application of such materials to displays, lighting, flexible thin film electronics, solar energy conversion and sensors. The field is a growth area, nationally and globally, evidenced by the rapidly expanding organic display and printed electronics industries. Organic semiconductors combine the semiconductor properties traditionally associated with inorganic materials with the more desirable properties of plastics. Moreover, the organic syntheses of these materials allow for great flexibility in the tuning of their electronic and optical properties. By combining these properties, organic semiconductors such as conjugated polymers have been demonstrated as the active material in light-emitting diodes (LEDs), transistors, and photovoltaic (PV) cells. Furthermore, these conjugated polymers provide a new way of looking at many of the broad fundamental scientific issues related to using molecules for electronics. A great deal of the physics which governs the behaviour of molecules for electronics occurs at the organic-organic interfaces (heterojunctions). For example, the nature of organic interfaces determines the fate of excitons to be either stabilised (for efficient LEDs) or destabilised (for efficient PV cells) at the interfaces. Therefore, by selecting semiconductors with proper band-edge offsets between their conduction and valence bands, different device characteristics can be readily achieved. While significant progress has been made in developing the materials and high performance organic devices, many fundamental aspects of organic-organic semiconductor interfaces remain to be understood. In particular, fundamental understanding of the correlation between nanostructures and interfaces of organic semiconductors in thin films and multilayers and associated device performance still remain to be fully explored. In this Chapter, we will introduce how to control and characterise various length-scale organic-organic interfaces facilitating the rational design of materials, device architectures and fabrication methods via increased understanding of fundamental properties of organic-organic interfaces and their modification due to processing. In particular, we will address the distinctive optoelectronic and charge transport properties which have been observed across different organic-organic interfaces depending on their length-scale (micron-scale in the blends down to molecular-scale in the copolymers) and nature (interchain vs intrachain), providing the deeper understanding of organic interfaces and their vital roles in various optoelectronic devices. The key advances in organic semiconductor interfaces achieved so

far will provide important insight into a design rule of organic semiconductors which is essential for future development in molecular electronic devices.

2. The main aim and contents of this chapter

This chapter aims to review fundamental scientific issues related to using molecules for electronics down to the single-molecule scale by studying a range of well-controlled organic-organic interfaces, with a particular focus on their role on electronic structures and electronic processes of organic semiconductors and their devices. Specific topics were:

1. Control and characterisation of various length-scale organic interfaces (Section 3)
2. Photophysical dynamics of electronic species at the organic interfaces (Section 4)
3. Electronic processes of charge carriers across the organic interfaces (Section 5)
4. Charge-carrier operational dynamics across the organic interfaces (Section 6)

3. Control and characterisation of various length-scale organic interfaces

3.1 Interfaces controlled by polymer molecular weight variation

Polymer molecular weight (MW) (i.e. chain length) variation was used as a tool to control the phase separation laterally and/or vertically in blend films (Yim et al., 2010). The conjugated polymers studied are poly(9,9-di-*n*-octylfluorene-*alt*-benzothiadiazole) F8BT ($M_n = 9 - 255$ kg/mol) and poly(9,9-di-*n*-octylfluorene-*alt*-(1,4-phenylene-((4-*sec*-butylphenyl) imino)-1,4-phenylene) TFB ($M_n = 3 - 102$ kg/mol) (Chemical structures in Table 1). Micron-scale lateral phase separation is observed in blend films that consist of high MW of both F8BT and TFB ($M_n > 60$ kg/mol), in which domain sizes increase with MW of each homopolymer. For these blend films, the micro-Raman spectroscopy study indicates that the higher-lying domains are F8BT-rich and the lower-lying domains are TFB-rich. In contrast, the blend films that consist of at least one low MW homopolymer ($M_n < 10$ kg/mol) show relatively smooth surface with sub-micron or no measurable lateral phase separation.

Using the surface-sensitive X-ray photoelectron spectroscopy (XPS) technique, it is observed first that, for blend films that consist of at least one low MW polymer ($M_n < 10$ kg/mol), there is a significant enrichment of the short polymer chains at the film-air interface. This reveals that the vertical phase segregation at the film-air interface is driven by the contrast of MW between the two homopolymers. On the other hand, for blend films that show micron-scale lateral phase separation, the film-air interface is always enriched with TFB, suggesting the presence of TFB capping layer apart from the exposed TFB-rich domains. Second, for all the blend films at the film-substrate interface, there is an enrichment of the lower surface energy material (TFB). The extent of TFB enrichment is found to increase with the MW of both polymers, possibly due to increased thickness or purity of the TFB wetting layer in these blend films. These observations suggest that surface energy contrast (as oppose to MW contrast) might be the dominant driving force in determining the vertical phase segregation at the film-substrate interface. Based on the morphological and compositional analyses of these blend films, we proposed two different models of the final phase separated structures (Fig 1a and 1b) for blend films without and with micron-scale lateral phase separation, respectively.

For the blend films with no visible lateral phase separation (in which a large MW contrast exists between the two homopolymers), the film-air interface is enriched with the low MW polymer, while the film-substrate interface is always enriched with the lower surface energy

polymer TFB. For the blend films with obvious micron-scale lateral phase separated structures, additional nanoscale vertical phase segregation also occurs resulting in a continuous TFB wetting layer at the film-substrate interface and a discontinuous TFB capping layer at the film-air interface (^aKim et al., 2004). These remarkably different lateral and vertical phase separation observed in the F8BT:TFB blend films has important implications on LED performance.

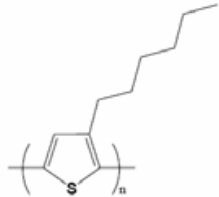
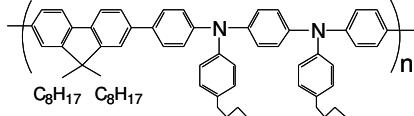
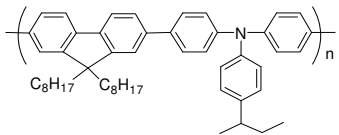
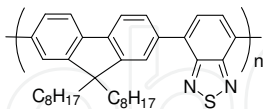
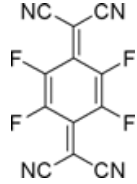
Material	Chemical Structure	HOMO [eV]	PL efficiency
P3HT		-4.8	0.1 0[a]
PFB		-5.1	0.65 0[a] 0.35[b]
TFB		-5.3	0.4 0.05[a] 0.1[b]
F8BT		-5.9	0.6 0.05[a]
F ₄ -TCNQ		-5.2[c]	-

Table 1. Chemical structures and optoelectronic properties of conjugated polymers and F₄TCNQ. ^[a] PL efficiency of 5 % F₄TCNQ-doped polymer, ^[b] PL efficiency of 5 % F₄TCNQ-doped polymer after annealing (N₂ environment, 200 °C, 1 hr), ^[c] LUMO level of F₄TCNQ

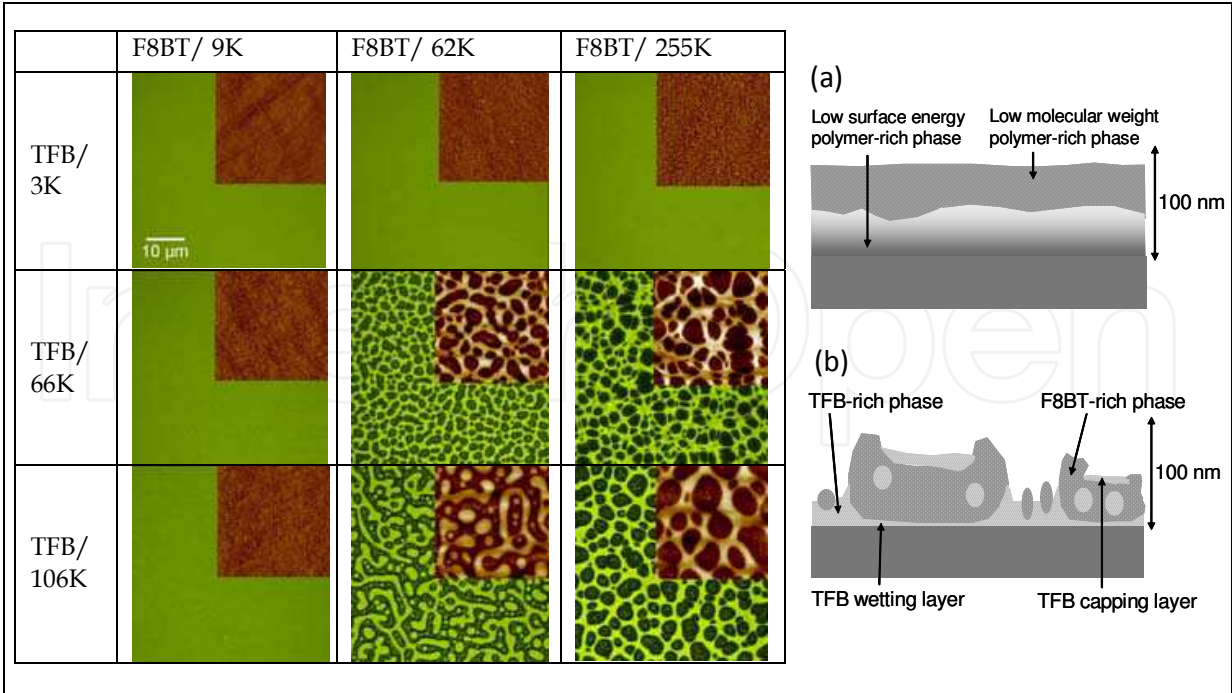


Fig. 1. Left: PL images of F8BT:TFB blend films (100nm, 1:1 by weight) with different MWs under blue excitation. The bright regions correspond to F8BT-rich phases while the dark regions TFB-rich phases. Inset: AFM images (20µmX20µm). Right: Proposed cross sections (a) at least one low MW homopolymers and (b) high MW of both homopolymers

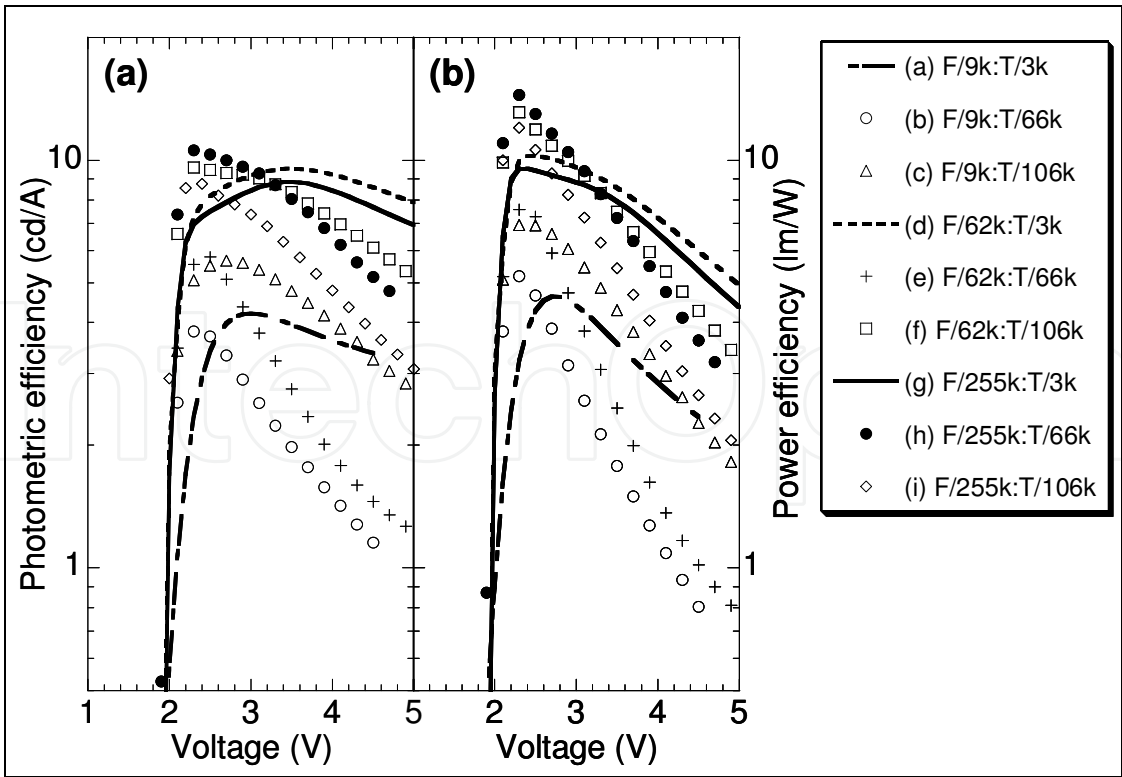


Fig. 2. EL efficiency-voltage characteristics of LEDs fabricated with F8BT:TFB blend films with different molecular weights of each copolymer, in (a) cd/A and (b) lm/W

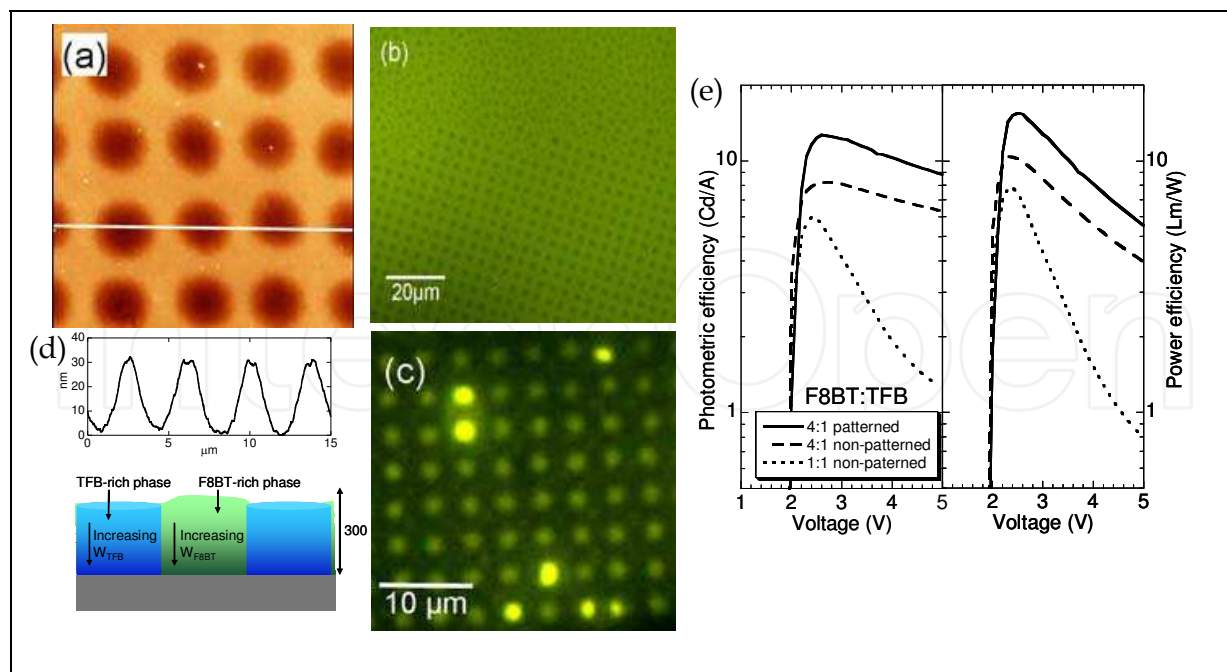


Fig. 3. (a) AFM image ($15\ \mu\text{m} \times 15\ \mu\text{m}$, on $70\ \text{nm}$ height scale) of the patterned F8BT:TFB blend film. Surface line scan (below) indicates that the height difference between the higher-lying F8BT-rich and lower-lying TFB-rich phases is $\sim 30\ \text{nm}$. (b) PL image of $\sim 300\ \text{nm}$ -thick patterned F8BT:TFB blend film under blue excitation ($2.85\ \text{eV}$). The bright and dark regions in the PL image correspond to F8BT-rich and TFB-rich phases, respectively. Note the contrast between the areas with and without the 2D pattern. (c) EL image of the patterned LED at 7V showing EL from enclosed TFB-rich domains. Differences in brightness between the TFB-rich domains might be due to thickness variation across the blend film. (d) Schematic drawing summarizes the proposed cross section of the patterned F8BT:TFB blend film based on micro-Raman compositional analysis. Both domains show increased purity of the corresponding polymer nearer to the patterned substrate. (e) EL efficiency-voltage characteristics of LED fabricated with the patterned blend film expressed in Cd/A and Lm/W . F8BT:TFB blend devices (4:1 and 1:1 by weight) prepared by spin-coating are included for comparison

The performance of LEDs fabricated with these blend films is found to be closely related to the blend thin film morphology, which varies remarkably with the molecular weight of both polymers (Figure 2). All the devices fabricated with the blend films exhibit sharp turn-on in both current and luminance at $\sim 2\ \text{V}$. Two distinctive efficiency-voltage characteristics are observed in these blend devices. First, blend films that exhibit micron-scale lateral phase separation show high initial efficiencies just after turn-on, but decreases rapidly at high voltages. Such device characteristics are closely related to the blend film morphology. While the continuous TFB wetting layer might assist hole injection/transport and act as electron blocking layer at the anode interface, the discontinuous TFB capping layer might localise electron injection from the cathode, resulting in a high degree of spatial confinement of charge carriers. This then leads to high electron-hole recombination efficiency at organic-organic interfaces (Morteani et al., 2003), which may explain the observed high initial EL efficiencies in these blend films. However, at high voltages, the presence of very thin lower-lying TFB-rich domains provide a pathway for holes to punch through the blend film

without undergoing radiative recombination with electrons, causing imbalance of charge carriers and hence an increase in leakage current and the rapid decay in EL efficiencies. Second, among the blend films with no observable micron-scale lateral phase separation, those that consist of TFB/3K show relatively lower peak initial efficiency, comparing to those with micron-scale lateral phase separation. This is attributed to the lack of phase separated features that can assist spatial confinement of charge carriers, as discussed earlier. However, improved film thickness uniformity and balance of charge carriers do contribute to reduce leakage current at high voltages, explaining the observed slower decay in EL efficiencies. Furthermore, the amount of surface out-coupling of light in the forward direction observed in blend devices is found to be positively correlated to the distribution of periodicity of the phase-separated structures in the active layer.

3.2 Interfaces controlled by patterned substrate

The phase separation in organic blend thin films can be controlled via chemical modification of the substrate with a periodic contrast of the substrate surface energy by microcontact printing (aYim et al., 2008). With appropriate choice of polymer molecular weight and blend ratio, the phase-separated structures in the blend film closely replicate the underlying 2D pattern since the low surface energy component TFB preferentially migrate away from regions of higher surface energy (Figure 3). Micro-Raman analysis revealed nanometer-scale vertical segregation of the polymers within both lateral domains, with regions closer to the substrate being substantially pure with each of the two polymers. This indicates the absence of a continuous TFB wetting layer typically formed in blend films spin-coated on non-patterned surfaces, and has important implications on device performance. It also implies the formation of periodic TFB/F8BT (and reversed) heterojunctions structures which favour (and suppress) charge carrier injection from both electrodes in the TFB-rich (F8BT-rich) domains. As a result, charge carrier injection is confined in the well-defined enclosed TFB-rich domains, leading to high EL efficiency. The overall reduction in the patterned blend film roughness as compared to reference spin-coated blend (1:1 by weight) leads to slower decay in EL efficiency at high voltages. The amount of surface out-coupling of light in the forward direction observed in blend devices is also found to be positively correlated to the distribution of periodicity of the phase-separated structures in the active layer.

3.3 Interfaces controlled by thin film transfer printing technique

The fabrication of functional multilayered conjugated polymer structures with well-defined organic-organic interfaces for optoelectronic device applications is constrained by the common solubility of many polymers in most organic solvents (bYim et al., 2008). A simple, low-cost, large-area transfer printing technique for the deposition and patterning of conjugated polymer thin films has been demonstrated. This method utilises a planar poly(dimethylsiloxane) (PDMS) stamp, along with a water-soluble sacrificial layer, to pick up an organic thin film (~20nm-1µm) from a substrate and subsequently deliver this film to a target substrate. The versatility of this transfer printing technique and its applicability to optoelectronic devices have been shown by fabricating bilayer structures of TFB/F8BT and poly(3-hexylthiophene) (P3HT)/ methanofullerene([6,6]-phenyl C₆₁ butyric acid methyl ester) (PCBM), and incorporating them into light-emitting diodes and photovoltaic cells, respectively (Figure 4). For both types of devices, bilayer devices fabricated with this transfer printing technique showed equal, if not superior performance to either blend

devices or bilayer devices fabricated by other techniques. This indicates well-controlled organic-organic interfaces achieved by the transfer printing technique.

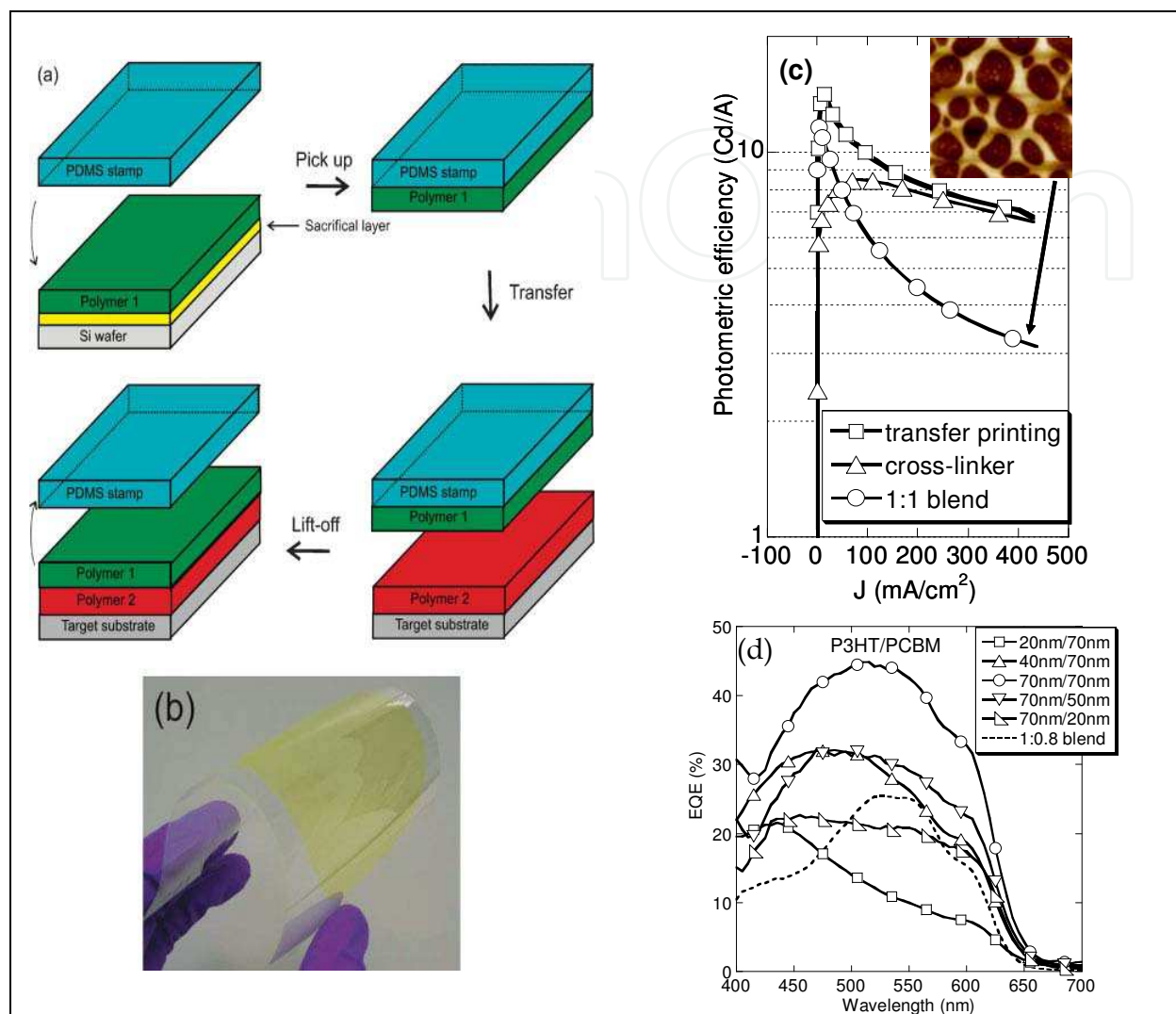


Fig. 4. (a) Schematic depiction of the thin film transfer printing process to form a bilayered conjugated polymer structure. (b) A photograph of a 4-inch transfer printed F8BT thin film (~ 70 nm) on a flexible PET sheet. (c) EL efficiency (Cd/A) as a function of diode current (J) of LEDs with TFB/F8BT bilayered films (20nm/80nm) fabricated by transfer printing technique (square) and cross-linker (triangle), and TFB:F8BT blend film (1:1 by weight, circle). (d) External quantum efficiency (EQE) of P3HT/PCBM bilayered solar cells fabricated by transfer printing technique, with different thicknesses of either P3HT or PCBM (20-70 nm), while keeping the thickness of the other material (70 nm) and other processing conditions constant. An EQE spectrum of a P3HT:PCBM blend device (1:0.8 by weight) is included for comparison

3.4 Interfaces controlled by copolymerization of electron donor and acceptor units

The molecular-scale intrachain interfaces (heterojunctions) can be created by copolymerization of TFB (electron donor) and F8BT (electron acceptor) polymers by covalently attaching them to a main conjugated polymer backbone (Kim et al., 2008) and

also by adding different amounts of the strongly electron accepting BT unit into the F8 polymer backbone, F8_{1-x}BT_x copolymers ($0 \leq x \leq 0.5$) (Winfield et al., 2009). We have observed that not only are excitons in F8_{1-x}BT_x copolymers ($0 \leq x \leq 0.5$) strongly charge transfer (CT) in character but that the strength of this CT character increases when the proportion of BT units in the polymer chains is small. Incorporation of the strongly electron-accepting BT unit, even in small proportions, into the F8 polymer chain results in localization of the lowest unoccupied molecular orbital (LUMO) on the BT units. There are no significant changes in the highest occupied molecular orbital (HOMO) and LUMO energies with BT content leading to the same shape of the F8BT emission in the PL spectrum for all F8_{1-x}BT_x copolymers. Increased coupling of the excited state to the ground state at higher BT content results in shorter exciton lifetime and higher PL efficiency. The increased CT character of the excitons in lower-BT content copolymers is also seen in the stronger solvent dependence of the emission spectra and excited state lifetimes of these copolymers.

4. Photophysical dynamics of electronic species at the organic interfaces

4.1 Photoinduced intrachain charge transfer state in copolymer

The optoelectronic properties at the organic-organic semiconductor interfaces formed between polymer chains (interchain) and within a polymer chain (intrachain) are studied (Kim et al, 2008). These interfaces are fabricated using (TFB [F8-tfb]) (electron-donor) and (F8BT [F8-BT]) (electron-acceptor) conjugated polymers, by blending them together or by covalently attaching them via a main polymer backbone (copolymer). When a bulky and twisted tfb molecule is incorporated into a rigid F8BT conjugated backbone, it disturbs the conjugation of F8BT polymer, leading to a blue-shift in the lowest absorption transition. However, by acting as an effective electron donor, it assists the formation of an intrachain singlet exciton that has a strong CT character, leading to a red-shifted and longer-lived emission than that of F8BT. An extremely efficient and fast energy transfer from tfb donor to BT acceptor is observed in the copolymer (<1 ps) compared to transfer from TFB to F8BT in the blend (tens of ps). This efficient energy transfer in the copolymer is found to be associated with its low fluorescence efficiency (40-45% vs 60-65% for blend) because of the migration of radiative singlet excitons to low-energy states such as triplet and exciplex states that are nonemissive or weakly emissive.

4.2 Dielectric switching of the nature of excited state in copolymer

In a conjugated random copolymer (RC) composed of electron donor (TFB) and electron acceptor (F8BT) units, the spectral evolution of an intrachain neutral singlet exciton toward a CT state in solvents of increasing polarity has been monitored by time-resolved photoluminescence and ultrafast transient absorption spectroscopy (Petrozza et al., 2010). The PL spectra of the RC solutions in different polarity of solvents are shown and compared to the F8BT spectra (Figure 5). Very diluted solutions in o-xylene, the RC emission shows ~16 nm red-shift with respect to that of F8BT, with its lifetime slightly longer than that of F8BT (2.6 ns for RC vs. 2 ns for F8BT). This suggests that as the TFB unit is covalently linked to the F8BT backbone, the emission in RC occurs from an electronic state of different nature compared to F8BT. The F8BT itself shows a red shift of ~30 nm in PL spectra as the polarity of the medium is increased from the o-xylene (dielectric constant, $\epsilon = 2.57$) to the o-dichlorobenzene ($\epsilon = 4.81$) solvents underlying the polar nature of the relaxed emissive state resulted from the localisation of the electron wavefunction on the BT unit. In the RC, this

solvatochromic effect is strongly amplified. There is a significant increase in the red-shift, ~ 114 nm shift going from the cyclohexane ($\epsilon = 2.02$) to the *o*-dichlorobenzene ($\epsilon = 9.93$) solution, and spectral changes in emission spectra. In addition, these spectral changes are accompanied by a concomitant enhancement of the luminescence lifetime (from 2.6 ns to 5.7 ns) and reduction of the PL quantum yield when the solvent polarity increases. The sensitivity of the emissive state to the solvent dielectric constant supports its strong CT character in the relaxed configuration.

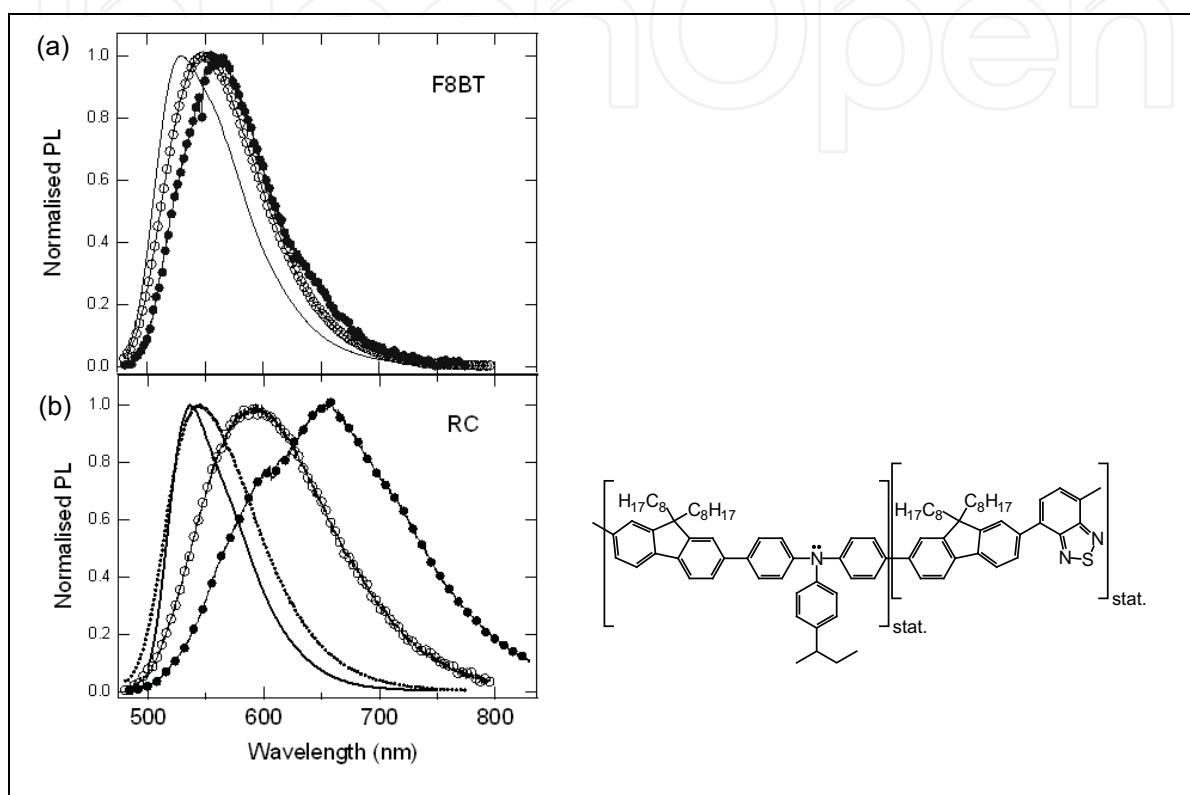


Fig. 5. PL spectra of diluted solutions of (a) F8BT and (b) RC in various solvents with different polarity, cyclohexane (solid line), *o*-xylene (dot line), chloroform (empty circles), *o*-DCB (filled circles). Excitation at 470 nm

In order to obtain further insight into the photophysical dynamics of the relaxation pathways, ultrafast transient absorption (TA) experiments have been performed. The TA spectra of F8BT in diluted *o*-xylene solution (Figure 6a) present two main features. For $\lambda < 600$ nm, a positive differential transmission signal ($\Delta T/T$) was observed. It is assigned to stimulated emission (SE) originating from the first excited singlet state, since its spectral position matches the fluorescence of the polymer. The SE could be observed over the entire detection time (about 2 ns). At $\lambda > 600$ nm, a photoinduced absorption (PA) band occurred which extended into the near infrared. This arises from the $S_1 \rightarrow S_n$ excited state absorption, since the SE and PA bands exhibited the same lifetimes and decay dynamics. A spectral broadening of the SE band was observed for *o*-xylene solution, whereas in the polar solvents (chloroform and *o*-DCB) a distinct dynamic red-shift of the band was observed (not shown). This is in agreement with the solvatochromic effect observed in the steady-state PL spectra and confirms the presence of a relaxed emissive state, which has a small polar character and is intrinsically sensitive to the environment.

The TA spectra of RC in *o*-xylene solution (Figure 6b) were found to be similar to the spectra of F8BT exhibiting a SE band below 620 nm and a PA band at longer wavelength. However, compared to the TA spectra of F8BT the SE band showed a dynamic red-shift and spectral broadening in the first 22 ps before decaying, indicating a stronger nuclear relaxation after photoexcitation. Fig. 6c shows the TA spectra of RC in chloroform solution. The SE and PA bands were observed at very early times (hundreds of fs). However, no spectral diffusion could be traced and within 3 ps the SE band evolved into a broad absorption band, which decayed slowly over the timescale of the experiment. The broad band shows a reduced PA response at 590 nm, which corresponds to the spectral region where the RC PL spectrum in chloroform solution peaks. This is ascribed to the competition between the SE and PA signal of the CT state. Similar spectral features have been observed in the *o*-DCB solution (Figure 6d), although they evolve considerably more slowly. Here, a complete relaxation of the SE band and a red-shift to about 590 nm in the first 25 ps have been observed followed by quenching of the SE band and the emergence of a broad absorption band to the infrared. It indicates that in polar solvents a charge-like absorption superimposes the region of stimulated emission and leads to a dramatic reduction in gain implying that CT states in the RC can be detrimental for light amplification and lasing.

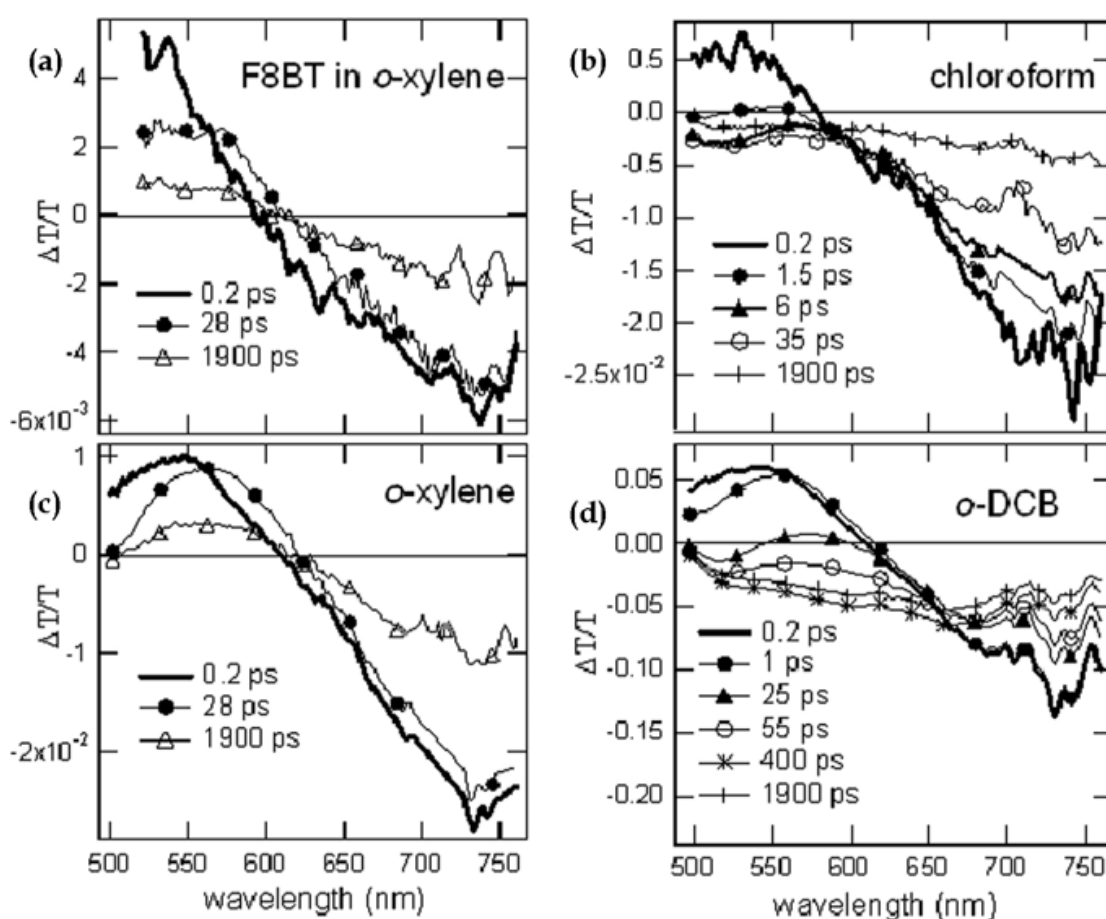


Fig. 6. Femto- to picosecond TA spectra of (a) F8BT in *o*-xylene solution and RC in (b) *o*-xylene, (c) chloroform, and (d) *o*-DCB solutions. TA spectroscopy was used to study the evolution and dynamics of the excited states on a timescale of hundreds of femtoseconds to milliseconds by probing the relative change in transmission ($\Delta T/T$) after photoexcitation at 490 nm

4.3 Intrachain versus intermolecular interactions at high pressure

The optical spectroscopy studies of F8BT polymers at high pressure have been performed in order to disentangle the intramolecular and intermolecular effects of hydrostatic pressure (Schmidtke et al., 2007). The PL spectrum of F8BT in a dilute solid state solution in polystyrene redshifts by ~320 meV over 7.4 GPa, while that of a F8BT thin film redshifts ~460 meV over a comparable pressure range. We attributed the redshift in solution to intrachain pressure effects, principally conformational planarization (i.e. a reduction in the torsional angle between the F8 and BT subunits of F8BT at high pressure). The additional contribution from interchain π -electron interactions accounts for the larger redshift of films.

4.4 Dynamic emission polarization anisotropy for aligned polymer films

Time-integrated and femtosecond time-resolved PL spectroscopy has been used to study the dynamic emission polarization anisotropy for aligned F8BT thin films (Schmid et al., 2008). The results indicate a high degree of chain alignment, with the presence of a small fraction of unaligned chain domains in film regions far from the imprinted surface. The time-averaged emission from aligned domains is found to be slightly shifted to higher photon energies compared to that from more disordered film regions. This effect is attributed to a subtly different chain packing geometry in the more aligned regions of the film, which leads to a reduced exciton diffusivity and inhibits energetic relaxation of the exciton in the inhomogeneously broadened density of states. While for an unaligned reference film, exciton migration results in a nearly complete depolarization of the emission over the first 300 ps. For the aligned films, interchain exciton hopping from unaligned to aligned domains is found to increase the anisotropy over the same time scale. In addition, excitons generated in aligned film domains were found to be slightly more susceptible to nonradiative quenching effects than those in disordered regions deeper inside the film, suggesting a marginally higher defect density near the nanoimprinted surface of the aligned film.

5. Electronic processes of charge carriers across the organic interfaces

5.1 Effects of polymer packing structure on optoelectronic properties

Spin-coated F8BT films of different molecular weights ($M_n = 9 - 255$ kg/mol), both in the pristine and annealed state, were studied in an effort to elucidate changes in the polymer packing structure and the effects this structure has on the optoelectronic and charge transport properties of these films (Donley et al., 2005; Zaumseil et al., 2006). A model based on quantum chemical calculations, wide-angle X-ray scattering, atomic force microscopy, Raman spectroscopy, photoluminescence, and electron mobility measurements was developed to describe the restructuring of the polymer film as a function of polymer chain length and annealing. In pristine high molecular weight films, the polymer chains exhibit a significant torsion angle between the F8 and BT units, and the BT units in neighboring chains are close to one another. Annealing films to sufficiently high transition temperatures allows the polymers to adopt a lower energy configuration in which the BT units in one polymer chain are adjacent to F8 units in a neighboring chain ("alternating structure"), and the torsion angle between F8 and BT units is reduced. This restructuring, dictated by the strong dipole on the BT unit, subsequently affects the efficiencies of interchain electron transfer and exciton migration. Films exhibiting the alternating structure show significantly lower electron mobilities than those of the pristine high molecular weight films, due to a decrease in the efficiency of interchain electron transport in this structure (Figure 7a). In addition, interchain exciton migration to low

energy weakly emissive states is also reduced for these alternating structure films, as observed in their photoluminescence spectra and efficiencies (Figure 7b).

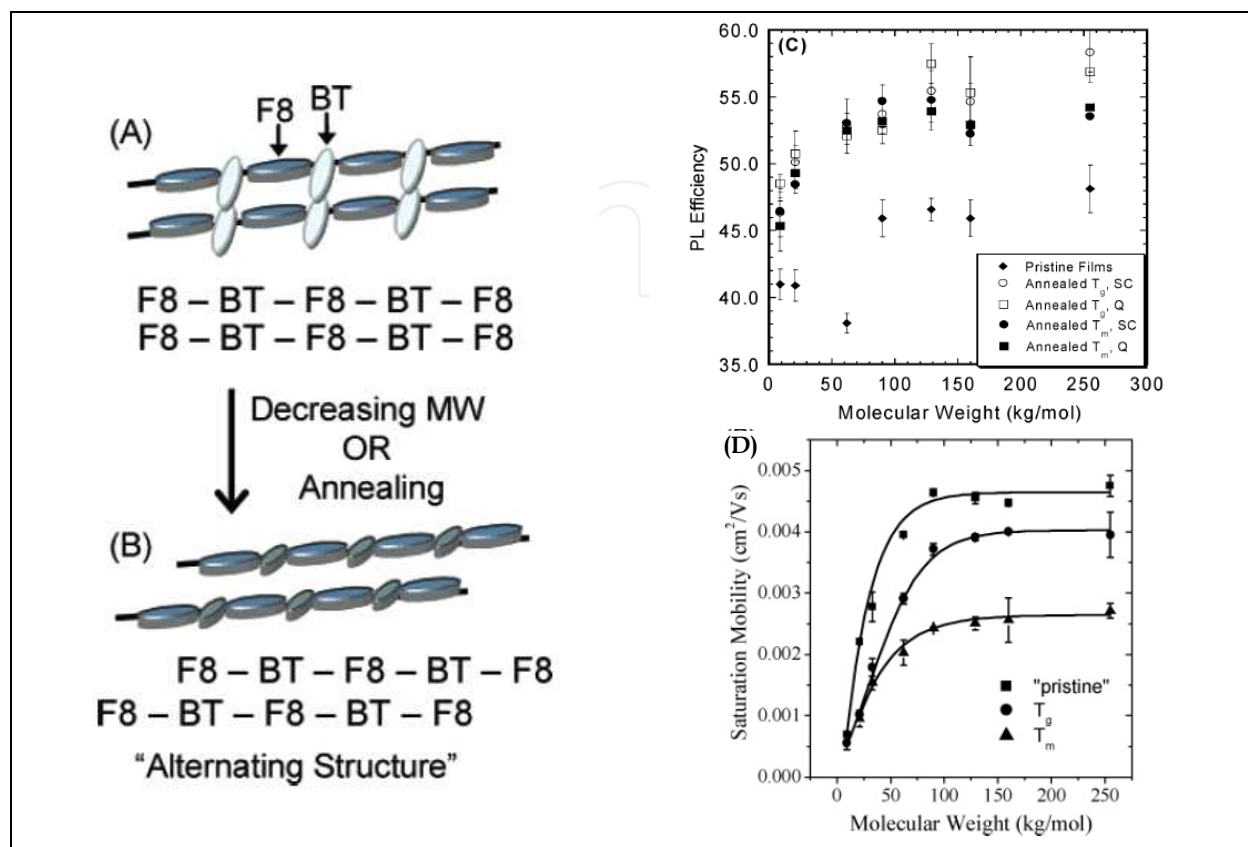


Fig. 7. Schematic illustrations showing (A) the initial packing structure of the high molecular weight pristine films. The BT units exhibit a relatively high torsion angle with respect to the F8 units, and in neighboring polymer chains, the BT units are adjacent to each other. (B) The packing structure for the low molecular weight pristine films or annealed films. Adjacent polymer chains have been translated with respect to one another, so that the BT units in one chain are adjacent to the F8 units in the neighboring chain (termed "alternating structure"). This structure forces the BT units into a geometry that is more planar with the F8 units. (C) PL efficiencies for pristine and annealed films. The sample with a molecular weight of 62 kg/mol is known to have some inorganic impurities and shows a low PL efficiency. (D) Electron mobilities calculated in the saturation region for F8BT films annealed to different temperatures. Decreases in mobility were observed upon annealing and for the shorter molecular weights. "Pristine" films are those that were heated only to 100 °C to remove residual solvent trapped in the films before further processing steps

5.2 Enhanced charge transport properties of aligned F8BT films by nanoconfinement

The uniaxial alignment of a liquid-crystalline conjugated polymer F8BT, by means of nanoconfinement during nanoimprinting has been demonstrated (Zheng et al., 2007). The orientation of the conjugated backbones was parallel to the nanolines imprinted into the polymer film. Polarized UV-vis absorption and photoluminescence spectra were measured to quantify the degree of alignment, showing that the polarization ratio and uniaxial molecular order parameter were as high as 66 and 0.97, respectively. The aligned F8BT film was used as

the active layer in a PLED, which resulted in polarized electroluminescence with a polarization ratio of 11. Ambipolar polymer FET in a top-gate configuration with aligned F8BT as the active semiconducting layer showed mobility enhancement when the chains were aligned parallel to the transport direction. Mobility anisotropies for hole and electron transports were 10-15 and 5-7 respectively, for current flow parallel and perpendicular to the alignment direction.

5.3 Intrachain versus interchain electron transport

F8BT displays very different charge-transport properties for holes versus electrons when comparing annealed and pristine thin films and transport parallel (intrachain) and perpendicular (interchain) to the polymer axes. We have performed a quantum-chemical calculation focusing on the electron-transport properties of F8BT chains and compared the efficiency of intrachain versus interchain transport in the hopping regime (Van Vooren et al., 2008). The theoretical results rationalize significantly lowered electron mobility in annealed F8BT thin films and the smaller mobility anisotropy ($\mu_{\parallel}/\mu_{\perp}$) measured for electrons in aligned films (i.e. 5-7 compared to 10-15 for holes).

5.4 Controlled electrical properties via a solution-based *p*-type doping

We have controlled *p*-doping of P3HT, PFB, TFB and F8BT conjugated polymers by co-blending with F₄TCNQ in a common organic solvent (Yim et al., 2008). Doping leads to significant increase in the bulk conductivity and hole current of the polymers with gradual disappearance of turn-on voltage. The effectiveness of doping increases as the HOMO level of the polymers becomes smaller, from F8BT (5.9eV) to P3HT (4.8eV), indicating that *p*-doping occurs via electron transfer from the HOMO level of the polymers to the LUMO level of F₄TCNQ (Figure 8). F₄TCNQ appears as a promising candidate to *p*-dope a wide range of conjugated polymers. This solution-based doping process will be one of the most effective and desirable ways to control the electrical properties of organic materials, in particular for solution processable organic semiconductors and their associated devices. In particular, a single polymer material can be used as both semiconductor and conductor in a single device.

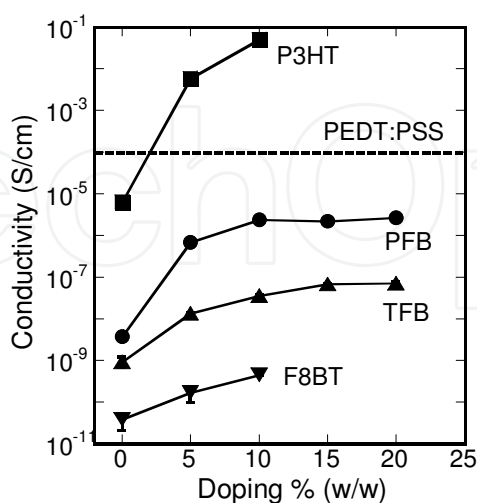


Fig. 8. Measured conductivity of the conjugated polymer films doped with different concentrations of F₄TCNQ. Polymer films were deposited on substrates with inter-digitated ITO structures. The applied electric field was $\leq 4 \times 10^{-4}$ V/nm. The conductivity of PEDT:PSS film typically used in organic devices is included for comparison

5.5 Improved PLED efficiency by inserting a thin polymer interlayer

It is demonstrated that adding a thin (10 nm) conjugated polymer interlayer between PEDT:PSS and an emissive semiconductor prevents the exciton quenching at the PEDT:PSS interface, resulting in a significant improvement in the device efficiency of polymer LEDs (Kim et al., 2005). For PLEDs with the TFB interlayer, the external quantum efficiency (EQE) increases from 0.7% (0.4 CdA at 3.7 V) to 1.9% (1.0 CdA at 3.3 V) at 100 Cd/m² for red LEDs and from 1.9% (6.2 Cd/A at 3.4 V) to 3.0% (10.1 Cd/A at 3.0 V) at 1000 Cd/m² for green LEDs. An EQE of 4.0% is also observed in blue LEDs (35% increase). The increase in the efficiency is accompanied by a large increase in the device lifetime (up to five times for red LEDs and four times for green LEDs). This thin-conjugated polymer interlayer is spin-coated from TFB solution directly on top of the PEDT:PSS layer. TFB is a triarylamine-based large-band-gap semiconductor (3.0 eV) often used as a hole transporter due to its low ionization potential (5.33 eV) and high hole mobility. One of the main roles of this TFB interlayer is considered to be a blocking layer that prevents the radiative excitons from direct quenching by PEDT:PSS and thus to remove a nonradiative decay channel introduced by PEDT:PSS. This exciton blocking property of the TFB interlayer contributes to improvement of the device performance. We demonstrate this by directly measuring the exciton lifetime, the time taken for an excited state to decay radiatively, of F8BT emissive semiconductor in direct contact with PEDT:PSS and TFB interlayer, using time-correlated single-photon counting technique (Figure 9).

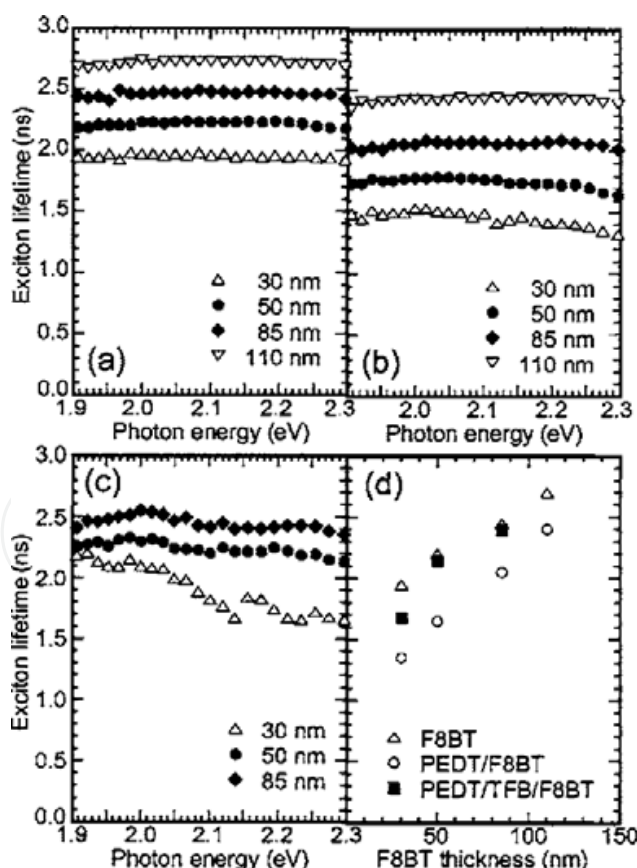


Fig. 9. Exciton lifetime of (a) F8BT, (b) PEDT:PSS/F8BT, (c) PEDT:PSS/TFB/F8BT films as a function of emitted photon energy, and (d) as a function of F8BT film thickness at 2.27 eV. PEDT:PSS is a poly(3,4-ethylenedioxythiophene) doped with poly(styrenesulphonate)

6. Charge-carrier operational dynamics across the organic interfaces

6.1 Effects of charge balance on transient electroluminescence

Charge balance inside the active layer has been studied by applying a pulse-mode electrical excitation to the device. The transient response of the devices under pulsed excitation yields important information related to charge injection and transport pathways (Seeley et al., 2004), in addition to its obvious use in high-brightness pulsed devices. In this study, a constant voltage pulse (4 μ s pulses with a repeat rate of 30 Hz) was sent to the devices and their transient EL characteristics were monitored (Kim et al., 2008). The device fabricated with a TFB (50nm)/ F8BT (50nm) bilayer was added for the pulse measurements in order to address the important role of different length-scale polymer-polymer interfaces in the charge-carrier transport and recombination processes. The pulsed measurements revealed a remarkably clear trend through the appearance of a “turn-on” spike in the EL output of the devices (Figure 10a). This “turn-on” spike was strongest in the bilayer device and gradually decreases as the length-scale of the organic interfaces decreases, starting with micron-scale in the blend and ending with molecular-scale in the RC. Therefore, no turn-on spike was observed in the RC. The turn-on spikes were not observed either in the neat F8BT or neat TFB devices.

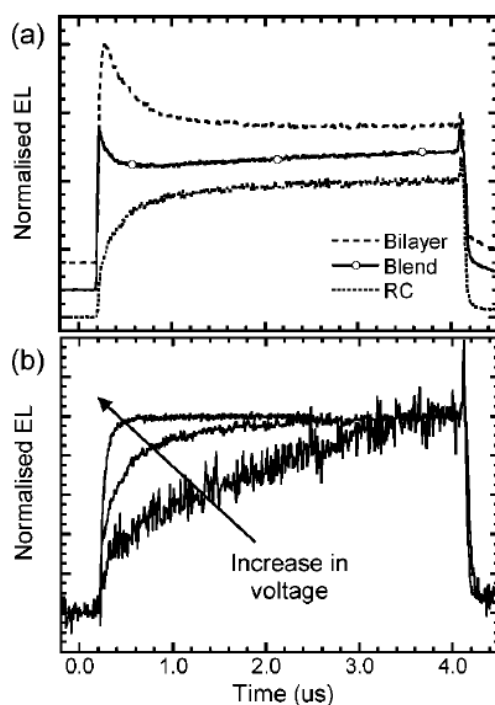


Fig. 10. (a) Pulsed measurements of TFB:F8BT LEDs fabricated with bilayer (50 nm TFB/50 nm F8BT), polymer blend, and RC. A constant voltage pulse (5.5 V for the blend and 11-12 V for others) with the duration of 4 μ s and 30 Hz repeat rate was used. (b) Pulsed measurements of the RC LED with an increase in the voltage from 6.5 V to 14.5 V

This turn-on spike can be understood by associating it with charge balance inside the active layer after an initial electrical excitation, although its exact origin has not yet been clearly established. An ohmic contact is formed at the cathode interface between F8BT and Ca electrode since the F8BT energy level for electron injection (i.e. LUMO level, \sim 2.95 eV) lies very closely to the work function of Ca electrode (\sim 2.9 eV). Hence once a contact is made,

there is no injection barrier for electrons and this provides a barrier-free injection of electrons into the F8BT layer even before the driving voltage is applied. Inside the bilayer device, this would lead to an accumulation of electrons at the interface between TFB and F8BT layers due to the energy barrier for electrons induced by the relatively low LUMO level of TFB (~ 2.25 eV). When a voltage pulse is applied, holes are injected into the TFB layer and meet the high density of electrons already accumulated at the TFB/F8BT interface to recombine and give rise to light emission, thus a sudden spike can appear in the EL. As time passes, the accumulated electrons quickly run out and the flow of opposite charges becomes more balanced and thus produces more constant EL.

In the blend device, μm length-scale TFB-rich phases are dispersed in a F8BT-rich matrix. This F8BT-rich matrix may provide a reasonable pathway for the electron injection and transport, leading to accumulation of barrier-free injected electrons upon contact with Ca cathode. Once the voltage pulse is applied, the flow of holes into the active layer would cause a similar but smaller turn-on spike as that seen in the bilayer. The smaller turn-on spike in the blend device can be understood since freely injected electrons are distributed more evenly throughout the whole active layer, differently from the bilayer device in which high density accumulation of electrons occurs at the abrupt TFB/F8BT interface. As the length scale of the TFB/F8BT interfaces decreases in the copolymer, no accumulation of electrons is expected. In the RC device, where no continuous pathway for the electron transport is present due to randomly distributed TFB and F8BT interfaces at a molecular-scale, no turn-on spike is observed. Note that the absence of the turn-on spike in the RC does not depend on the voltage applied (Figure 10b). This observation agrees well with the single-carrier device data, confirming a better charge balance in the RC which produces more stable characteristics of LEDs in terms of device efficiencies.

6.2 Intrinsic and extrinsic degradation mechanisms

Understanding the diversity of steady-state operational mechanisms focusing on the electrochemical reaction pathways of injected charges across the organic semiconductor interfaces is very important to improve device efficiency and stability. However, there has been little work to address intrinsic and extrinsic mechanisms governing the electrical stability of these devices primarily due to the challenge of tracking minute chemical reactions *in-situ* in the 100-nm-thick buried active layers of polymer LEDs during operation. Work with micro-Raman spectroscopy has given very encouraging results in this field (Winfield et al., 2010; Ballantyne et al., 2010), in particular for degradation of the active layer of PLED devices (Kim et al., 2002; Kim et al., 2004).

We have also monitored *in-situ* changes to the chemistry of the polymers and their interfaces in the devices using non-destructive Raman spectroscopy. Fig. 11(a) shows an optical micrograph of an encapsulated polymer LED. It shows a $2\text{-}\mu\text{m}$ -wide pinhole defect surrounded by a diffusion disk on the ITO area. The pinhole and associated disk (which appears black under EL and therefore termed “black spot”) are marked by an optically distinct boundary. Fig. 11(b) shows the Raman spectra taken across this black spot. Our results confirm that the black spots are associated with cathode pinhole defects and caused by electrochemical activity between the cathode and hole-transport conducting polymer PEDT:PSS layer. We have also performed *in-situ* Raman measurements in hole-only poly(9,9-dioctylfluorene-co-bis-N,N-(4-butylphenyl)-bis-N,N-phenyl-1,4-phenylenediamine) (PFB) diodes to study a hole mediated interfacial reaction pathway during electrical

operation. The results suggest that a primary reaction pathway of the electrical properties of these diodes is the slow quasi-irreversible interfacial electrochemical oxidation (doping) of PFB adjacent to the PEDT:PSS layer (Figure 11c). Understanding such failure mechanisms under device operational conditions leads to the development of materials and devices that are intrinsically more resistant to degradation.

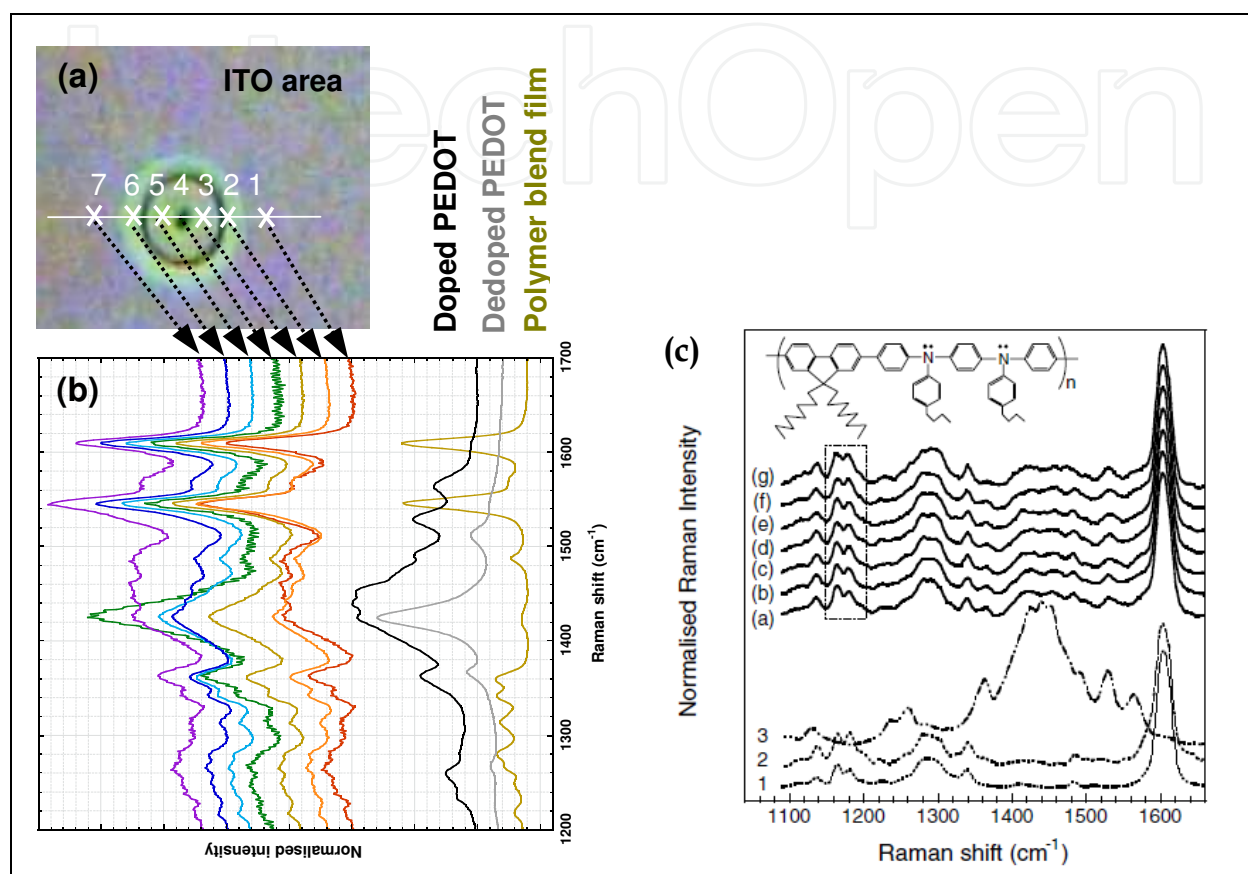


Fig. 11. (a) Enlarged optical micrograph of the black spot (ITO area), (b) Raman spectra taken across this black spot along the dotted line. All the spectra were normalised to the 1609 cm^{-1} peak of the EL polymer blend. Reference spectra for the EL polymer blend, doped-PEDOT:PSS and dedoped-PEDT:PSS, and (c) Raman spectra of the ITO/PEDT:PSS (60 nm)/PFB (100 nm)/Al (400 nm) diode after the J-V test at each point in Fig. 1A (excitation, 633 nm; objective NA, 0.7; spectra accumulation, 10_20 s). Reference spectra of (1) PFB, (2) electrochemically oxidised PFB, and (3) doped PEDT:PSS thin films are also shown. All the spectra except PEDT:PSS are normalised to the PFB Raman intensity at 1602 cm^{-1} . The chemical structure of PFB is also shown

6.3 In-situ identification of a luminescence quencher in OLEDs

In-situ Raman spectroscopy was also used to identify a luminescence quencher formed during OLED operation. Raman spectroscopy revealed that oxo-bridged dimerization occurs during the operation of $[\text{Ru}(\text{bpy})_3]^{2+}(\text{PF}_6^-)_2$ devices, where bpy is 2,2'-bipyridine. Photoluminescence spectroscopy showed that oxo-bridged dimers such as $[\text{Ru}(\text{bpy})_2(\text{H}_2\text{O})]_2\text{O}^{4+}(\text{PF}_6^-)_4$ effectively quench photoluminescence. Comparison of the Raman spectra from devices with the spectra from prepared blended films of $[\text{Ru}(\text{bpy})_3]^{2+}(\text{PF}_6^-)_2$ and

[Ru(bpy)₂(H₂O)]₂O⁴⁺(PF₆⁻)₄ demonstrated that sufficient dimerization occurs in the device to account for the luminescence quenching observed upon device driving. Dimerization occurred particularly where oxygen and moisture could penetrate the organic film. Dimerization could be a general failure mode of organic electroluminescent devices that incorporate metal complexes. Understanding failure under device-relevant conditions can lead to the development of materials and devices that are intrinsically more resistant to degradation (Slinker et al., 2007; Soltzberg et al., 2006).

7. Conclusion

In this chapter, we have reviewed our recent work carried out to understand the role of different length-scale organic-organic interfaces with an important focus on molecular-scale electronic structures and electronic processes across these interfaces. We have fabricated various length-scale interchain and intrachain organic interfaces using polymer blends with different molecular weight homopolymers and copolymers. We have also used surface patterning and transfer printing techniques to control length-scale of the organic interfaces. At these various interfaces, we have studied in depth the photophysical processes and dynamics of electronic species including intrachain charge transfer states and the transport and recombination of charge carriers. The distinctive optoelectronic and charge transport properties have been observed across different organic-organic interfaces depending on their length-scale (micron-scale in the blends down to molecular-scale in the copolymers) and nature (interchain vs intrachain), providing the fundamental understanding of these interfaces and their vital roles in various optoelectronic devices. Furthermore, based on the studies of charge carrier operational dynamics at these organic interfaces, we have been able to identify failure mechanisms of organic devices including intrinsic and extrinsic degradation mechanisms. The key advances in organic-organic semiconductor interfaces achieved so far will provide important insight into a design rule of organic semiconductors which is essential for future development in molecular electronic devices.

8. Acknowledgements

We thank Dr K. H. Yim, Dr A. Petrozza, Dr C. Donley, Dr. J. Winfield, Prof. H. Sirringhaus, Prof. Sir R. H. Friend, Dr. Z. Zheng, Prof. W. T. S. Huck, Prof. W. R. Salaneck, Dr. J. Cornil, Dr. D. Beljonne, Prof. G. G. Malliaras, Dr J. H. Burroughes for collaborations, and Cambridge Display Technology (CDT) Ltd. for materials supply. We thank the EPSRC-NPL Post-Doctoral Research Partnership Grant (EP/G062056/1) and the World Class University (WCU) Program through the National Research Foundation of Korea funded by the Ministry of Education, Science and Technology (Grant No. R32-10051).

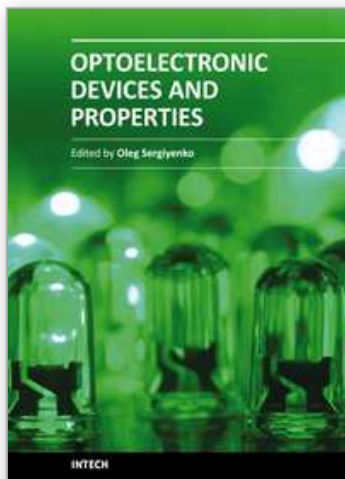
9. References

- Ballantyne, A.; Ferenczi, T.; Campoy-Quiles, M.; Clarke, T.; Maurano, A.; Wong, K.; Stingelin, N.; Kim, J. S.; Bradley, D.; Durrant, J.; McCulloch, I.; Zhang, W.; Heeney, M.; Nelson, J.; Mueller, C.; Smith, P.; Tierney, S.; Duffy, W. (2010). Towards Understanding The Influence of Morphology on Poly(3-hexylselenothiophene): PCBM Solar Cells. *Macromolecules*, 43, 1169-1174

- Donley, C. L., Zaumseil, J., Andreasen, J. W., Nielsen, M. M., Sirringhaus, H., Friend, R. H. and Kim, J. S. (2005). Effects of Packing Structure on the Optoelectronic and Charge Transport Properties in Poly (9,9-Dioctylfluorene-co-Benzothiadiazole). *J. Am. Chem. Soc.*, 127, 12890-12899
- ^aKim, J. S., Ho, P. K. H., Murphy, C. E. and Friend, R. H. (2004). Phase separation in polyfluorene-based conjugated polymer blends: Lateral and vertical compositional analysis of the blend thin films. *Macromolecules*, 37, 2861-2871
- ^bKim, J. S., Ho, P. K. H., Murphy, C. E., Seeley, A. J. A. B., Grizzi, I., Burroughes, J. H. and Friend, R. H. (2004). Electrical degradation of triarylamine-based LEDs monitored by micro-Raman spectroscopy. *Chem. Phys. Lett.*, 386, 2-7
- Kim, J. S., Grizzi, I., Burroughes, J. H., and Friend, R. H. (2005). Spin-cast thin semiconducting polymer interlayer for improving device efficiency of polymer light-emitting diodes. *Appl. Phys. Lett.*, 87, 023506
- Kim, J. S., Lu, L., Sreearunothai, P., Seeley, A., Yim, K. H., Petrozza, A., Murphy, C. E., Beljonne, D., Cornil, J., Friend, R. H. (2008). Optoelectronic and Charge Transport Properties at Organic/Organic Semiconductor Interfaces: Comparison Between Polyfluorene-Based Polymer Blend and Copolymer. *J. Am. Chem. Soc.*, 130, 13120-13131
- Morteani, A. C., Dhoot, A. S., Kim, J. S., Silva, C., Greenham, N. C., Friend, R. H., Murphy, C., Moons, E., Cina, S., Burroughes, J. (2003). Barrier-free electron-hole capture in polymer blend heterojunction light-emitting diodes. *Adv. Mater.* 15, 1708-1712
- Petrozza, A., Laquai, F., Kim, J. S. and Friend, R. H. (2010). Dielectric Switching of the Nature of Excited Singlet State in a Donor-Acceptor-type Polyfluorene Copolymer. *Phys. Rev. B*, 81, 205421
- Schmid, S. A., Yim, K.H., Chang, M. H., Kim, J. S., Friend, R. H. and Herz, L. M. (2008). Polarization anisotropy dynamics for thin films of a conjugated polymer aligned by nanoimprinting. *Phys. Rev. B*, 77, 115338
- Schmidtke, J. P., Kim, J. S., Gierschner, J., Silva, C. and Friend, R. H. (2007). Optical spectroscopy of a polyfluorene copolymer at high pressure: intra- and inter-molecular interactions. *Phys. Rev. Lett.*, 99, 167401
- Seeley, A. J. A. B., Friend, R. H., Burroughes, J. H. and Kim, J. S. (2004). Trap-assisted hole injection and quantum efficiency enhancement in poly(9,9' dioctylfluorene-co-benzothiadiazole) polymer light-emitting diodes. *J. Appl. Phys.*, 96, 7643-7649
- Slinker, J. D., Kim, J. S., Flores-Torres, S., Delcamp, J. H., Abruna, H. D., Friend, R. H. and Malliaras, G. G. (2007). In situ identification of a luminescence quencher in an organic light-emitting device. *J. Mater. Chem.*, 17, 76-81
- Soltzberg, L.J., Slinker, J.D., Flores-Torres, S., Bernards, D.A., Malliaras, G.G., Abruna, H.D., Kim, J.S., Friend, R.H., Kaplan, M.D., Goldberg, V. (2006). Identification of a Quenching Species in Ruthenium Tris-Bipyridine Electroluminescent Devices. *J. Am. Chem. Soc.* 128, 7761-7764
- Van Vooren, A., Kim, J. S., Cornil, J. (2008). Intrachain versus Interchain Electron Transport in Poly(fluorine-*alt*-benzothiadiazole): Quantum-Chemical Insight. *ChemPhysChem*, 9, 908-993
- Winfield, J. M., Van Vooren, A., Park, M. J., Hwang, D. H., Cornil, J., Kim, J. S., and Friend, R. H. (2009). Charge-transfer character of excitons in poly[2,7-(9,9-di-n-octylfluorene)_(1-x)-co-4,7-(2,1,3- benzothiadiazole)_(x)]. *J Chem. Phys.*, 131, 035104

- Winfield, J. M., Donley, C. L., Friend, R. H. and Kim, J. S. (2010). Probing thin-film morphology of conjugated polymers by Raman spectroscopy *J. Appl. Phys.*, 107, ISSN: 0021-8979
- ^aYim, K. H., Zheng, Z., Friend, R. H., Huck, W. T. S., and Kim, J. S. (2008). Surface-directed phase separation of conjugated polymer blends for efficient light-emitting diodes. *Adv. Funct. Mater.* 18, 2897
- ^bYim, K. H., Zheng, Z., Liang, Z., Friend, R. H., Huck, W. T. S. and Kim, J. S. (2008). Efficient Conjugated Polymer Optoelectronic Devices Fabricated by Thin Film Transfer Printing. *Adv. Funct. Mater.*, 18, 1012-1019
- ^cYim, K. H., Whiting, G., Murphy, C.E., Halls, J. J.M., Burroughes, J. H., Friend, R. H., and Kim, J. S. (2008). Controlling electrical properties of conjugated polymers via a solution-based p-type doping. *Adv. Mater.*, 20, 3319-3324
- Yim, K. H., Doherty, W. J., Salaneck, W. R., Murphy, C. E., Friend, R. H. and Kim, J. S. (2010) Controlling Phase Separation for Efficient Polymer Blend Light-Emitting Diodes, *Nano Lett.*, 10, 385
- Zaumseil, J., Donley, C. L., Kim, J. S., Friend R. H. and Sirringhaus, H. (2006). Efficient Top-Gate, Ambipolar, Light-Emitting Field-Effect Transistors Based on a Green-Light-Emitting Polyfluorene. *Adv. Mater.*, 18, (2006), 2708 – 2712
- Zheng, Z., Yim, K. H., Saifullah, M. S. M., Welland, M. E., Friend, R. H., Kim, J. S. and Huck, W. T. S. (2007). Uniaxial Alignment of Liquid-Crystalline Conjugated Polymers by Nanoconfinement. *Nano Lett.*, 7, 987-992

IntechOpen



Optoelectronic Devices and Properties

Edited by Prof. Oleg Sergiyenko

ISBN 978-953-307-204-3

Hard cover, 660 pages

Publisher InTech

Published online 19, April, 2011

Published in print edition April, 2011

Optoelectronic devices impact many areas of society, from simple household appliances and multimedia systems to communications, computing, spatial scanning, optical monitoring, 3D measurements and medical instruments. This is the most complete book about optoelectromechanic systems and semiconductor optoelectronic devices; it provides an accessible, well-organized overview of optoelectronic devices and properties that emphasizes basic principles.

How to reference

In order to correctly reference this scholarly work, feel free to copy and paste the following:

Ji-Seon Kim and Craig Murphy (2011). Organic-Organic Semiconductor Interfaces for Molecular Electronic Devices, Optoelectronic Devices and Properties, Prof. Oleg Sergiyenko (Ed.), ISBN: 978-953-307-204-3, InTech, Available from: <http://www.intechopen.com/books/optoelectronic-devices-and-properties/organic-organic-semiconductor-interfaces-for-molecular-electronic-devices>

INTECH
open science | open minds

InTech Europe

University Campus STeP Ri
Slavka Krautzeka 83/A
51000 Rijeka, Croatia
Phone: +385 (51) 770 447
Fax: +385 (51) 686 166
www.intechopen.com

InTech China

Unit 405, Office Block, Hotel Equatorial Shanghai
No.65, Yan An Road (West), Shanghai, 200040, China
中国上海市延安西路65号上海国际贵都大饭店办公楼405单元
Phone: +86-21-62489820
Fax: +86-21-62489821

© 2011 The Author(s). Licensee IntechOpen. This chapter is distributed under the terms of the [Creative Commons Attribution-NonCommercial-ShareAlike-3.0 License](https://creativecommons.org/licenses/by-nc-sa/3.0/), which permits use, distribution and reproduction for non-commercial purposes, provided the original is properly cited and derivative works building on this content are distributed under the same license.

IntechOpen

IntechOpen